

Evaluation of Acrylonitrile/Butyl Methacrylate/Halloysite Nanoclay Impregnated Wood Polymer Nanocomposites

Md. Rezaur Rahman,^a Josephine Chang Hui Lai,^{a,*} and Sinin Hamdan^b

Acrylonitrile/butyl methacrylate/halloysite nanoclay wood polymer nanocomposites (AN-co-BMA-HNC WPNCs) were prepared *via* the impregnation method, and the effect of different ratios of polymers was investigated. The WPNCs were characterized through weight percent gain, Fourier transform infrared spectroscopy (FT-IR), scanning electron microscopy (SEM), the three-point flexural test, dynamic mechanical thermal analysis (DMTA), thermogravimetric analysis (TGA), differential scanning calorimetry (DSC) analysis, and the moisture absorption test. The weight percent gain in the 50:50 AN-co-BMA-HNC WPNCs was the highest compared with the raw wood (RW) and other WPNCs. The FT-IR results confirmed that polymerization took place in the nanocomposites, especially in the 50:50 AN-co-BMA-HNC WPNCs, with a reduction of hydroxyl groups. The SEM results revealed that the 50:50 AN-co-BMA-HNC WPNCs showed the best surface morphology. The 50:50 AN-co-BMA-HNC WPNCs showed the highest flexural strength and modulus of elasticity. The results revealed that the storage modulus and loss modulus of the AN-co-BMA-HNC WPNCs were higher, while the $\tan \delta$ of the AN-co-BMA-HNC WPNCs was lower, compared with the RW. The AN-co-BMA-HNC WPNCs also exhibited higher thermal stability and exhibited remarkably lower moisture absorption compared with the RW. Overall, this study demonstrated that the 50:50 AN-co-BMA ratio was the most suitable to be introduced into RW.

Keywords: Morphology; Strength; Thermal; Clay

Contact information: a: Department of Chemical Engineering and Energy Sustainability, Faculty of Engineering, Universiti Malaysia Sarawak (UNIMAS), 94300 Kota Samarahan, Sarawak, Malaysia;

b: Department of Mechanical and Manufacturing Engineering, Faculty of Engineering, Universiti Malaysia Sarawak (UNIMAS), 94300 Kota Samarahan, Sarawak, Malaysia;

* Corresponding author: josephinelai91@hotmail.com

INTRODUCTION

Wood is used as a raw material in many technical and artistic applications (Vorreiter 1949). Wood fiber is widely used as a filler in composites because of its abundance and low cost (Bodîrlău *et al.* 2009)

In recent years, wood-based renewable nanocomposites, especially wood polymer nanocomposites (WPNCs), have gained a lot of attention from both scientific and commercial sectors. This is because the wood-based nanocomposites are lightweight, eco-friendly, and low-cost. Also, wood fibers are considered to be an alternative to glass or carbon fibers because of their environmental friendliness, biodegradability, and their low cost (Ashori 2008). WPNCs are materials composed of lignocellulosic fibers and thermoplastic polymers in varying percentages (Stark and Matuana 2007). WPNCs offer interesting improvement to various properties. Also, the introduction of wood fiber, which acts as a reinforcing filler in WPNCs, has great advantages, such as higher specific strength

and better toughness (Pakeyangkoon and Ploydee 2013). However, the application of wood fiber in nanocomposite materials is limited because of the hydroxyl groups inside the wood, which leads to poor compatibility with the hydrophobic polymer matrix (Kallakas *et al.* 2015). With poor compatibility, the properties of the WPNCs cannot be enhanced. Impregnation of wood is carried out to alter the structure of pure wood, as well as to improve the interfacial adhesion between the polymer matrix and wood fibers. This can lead to the improvement of the physical and mechanical properties of the WPNCs (Těšínova 2011).

Sindora wood is one wood species that is abundantly available in Malaysia. It is widely used in the production of furniture, agriculture implements, and heavy construction (Larsen *et al.* 1984). However, research into WPNCs with Sindora wood is still limited in both research and industry areas.

One of the polymer matrices that is often used in WPNCs includes acrylonitrile or polyamide. Acrylonitrile usually works with different polymer matrices to enhance the mechanical and thermal properties of WPNCs (Prochoń *et al.* 2007). Butyl methacrylate is usually applied in WPNCs for better thermal properties. It can be well intercalated with different fillers, such as silica or clay in small quantities (Kobayashi *et al.* 2002). Montmorillonite clay usually acts as a filler for WPNCs. It helps to produce a smooth finishing surface, lowers water absorption, and improves mechanical properties (Mekhemer *et al.* 2006).

The addition of silica into *in situ* emulsion polymerization of acrylonitrile-methyl methacrylate copolymers improves the thermal properties of the WPNCs (Bao *et al.* 2013). Poly(acrylonitrile-co-methyl methacrylate) copolymers undergo the precipitation polymerization technique, which remarkably improves the thermal stability, as well as the surface morphology of the nanoparticles (Eldin *et al.* 2014). The presence of nanoclay improves the modulus of elasticity of acrylonitrile-butadiene-styrene (ABS) nanocomposites through melt compounding (Singh and Ghosh 2014).

The presence of different clay loadings through *in situ* polymerization into the poly(styrene-co-butyl methacrylate) copolymer matrix can greatly improve the thermal properties (Siddiqui *et al.* 2013). The addition of surface-modified natural montmorillonite improves mixing between the clay and poly(n-butylacrylate) matrix through *in situ* polymerization, as well as the thermal properties of the nanocomposites (Herrera-Alonso *et al.* 2010).

The melt blended acrylonitrile-butadiene-styrene (ABS)/organically modified nanocomposites showed the presence of intercalated structure, as well as good dispersion of clay layers at low levels of its loading. However, the flexural strength properties decreased with the increase of nanoclay content (Aalaie and Rahmatpour 2007). In addition, ABS/nanoclay nanocomposites showed that the tensile strength was optimum at 2% while the dependency of hardness to the nanoclay content could achieve maximum up to 4% (Shishavan *et al.* 2014). The introduction of nanoclay into poly-ABS toughened polyoxymethylene (POM) improved the thermal stability and the tensile strength. The nanocomposites showed better properties compared to the pristine polymer. However, the elasticity of the nanocomposites decreased with the increasing amount of clay (Das *et al.* 2014). However, there has been no detailed work on the combination of a special polymer matrix, such as acrylonitrile-co-butyl methacrylate-halloysite nanoclay (AN-co-BMA-HNC), and wood fiber to produce a WPNC. Therefore, the aim of the present study was to fabricate AN-co-BMA-HNC WPNCs *via* the impregnation method and to investigate the

effect of different ratios of the polymer matrix on the physical, mechanical, morphological, and thermal properties of WPNCs.

EXPERIMENTAL

Materials

Defect-free and straight-grained *Sindora glabra* wood (RW) was obtained from Lundu, Sarawak, Malaysia. Both the control and modified wood samples were obtained from the same timber and machined at the same time with dimensions of 30 cm x 2 cm x 1 cm. The chemicals used to produce the WPNCs were acrylonitrile (AN), butyl methacrylate (BMA), benzoyl peroxide, and halloysite nanoclay (HN). The acrylonitrile and halloysite nanoclay was supplied by Sigma Aldrich (St. Louis, USA), while the butyl methacrylate and benzoyl peroxide were supplied by Merck Millipore (St. Charles, USA). The halloysite nanoclay was a nanopowder with particle diameters of 30 to 70 nm and lengths between 1 and 3 μm .

Methods

Preparation of acrylonitrile/butyl methacrylate/halloysite nanoclay wood polymer nanocomposites (AC-co-BMA-HNC WPNCs)

The polymer system was prepared using AN-co-BMA-HNC in the presence of benzoyl peroxide. The benzoyl peroxide acted as an initiator to influence the reaction between acrylonitrile and butyl methacrylate. Acrylonitrile, butyl methacrylate, and halloysite nanoclay were mixed in various ratios, given in Table 1. The mixtures were covered with aluminium foil and placed in an autoclave for 15 min to complete the reaction.

Table 1. Preparation of Polymer System in Various Ratios

Volume of acrylonitrile (AC) (mL)	Volume of butyl methacrylate (BMA) (mL)	Amount of halloysite nanoclay (HNC) (g)	Amount of benzoyl peroxide (g)	Sample's Code
0	200	2	5	AN-HNC WPNCs
100	100	2	5	50:50 AN-co-BMA-HNC WPNCs
140	60	2	5	70:30 AN-co-BMA-HNC WPNCs
200	0	2	5	BMA-HNC WPNCs

Impregnation of AN-co-BMA-HNC WPNCs

Four wood samples were prepared according to ASTM D1037 (2012) and were weighed using an electronic balance. The samples were then placed in the vacuum chamber

(box). The mixtures were poured into the vacuum box with a pressure of 0.1 bar for 60 min. After impregnation, the excess solution was removed from the wood samples with tissue paper. The wood samples were wrapped with aluminium foil and kept in an oven at 100 °C for 24 h for polymerization and the formation of the WPNCs. After polymerization, the aluminium foil was removed and the WPNCs were dried at 105 °C until a constant weight was obtained. The weight percent gain (WPG) of the WPNCs was then determined using Eq. 1,

$$\text{WPG} = \frac{W_f - W_o}{W_o} \times 100\% \quad (1)$$

where W_f is the oven-dried weight (gm) after impregnation of the WPNCs and W_o is the oven-dried weight (gm) before impregnation of the WPNCs.

Microstructural Characterization

Fourier transform infrared spectroscopy (FT-IR)

The infrared spectra of the WPNCs were recorded on a Shimadzu IRAffinity-1 (Tokyo, Japan). The technique used was attenuated total reflection (ATR). The transmittance range of the scan was 4000 to 600 cm^{-1} .

Scanning electron microscopy (SEM)

The interfacial bonding between the acrylonitrile, the butyl methacrylate, and the halloysite nanoclay was examined using a scanning electron microscope (SEM) (JSM-6710F, JEOL Company Limited, Akishima, Japan). The AN-co-BMA-HNC WPNCs were cut to dimensions of 5 mm x 5 mm x 5 mm (length x width x height). The accelerating voltage of this instrument was 15 kV. The specimens were first fixed with Karnovsky's fixative, and then put through a graded alcohol dehydration series. Once dehydrated, the specimen was coated with a thin layer of gold using gold sputter machine before being viewed microscopically. The micrographs were taken at magnifications ranging from 500 to 1000.

Three-point flexural test

The static flexural tests of the AN-co-BMA-HNC WPNCs were carried out using AG-X Plus Series Precision Universal Testers (300 kN Floor Model, Shimadzu Corporation, Tokyo, Japan). The dimensions of the flexural test specimens were 80 mm (length) x 30 mm (width) x 10 mm (thickness). The flexural tests were conducted according to ASTM D 790-03 (2003) at a cross head speed of 10 mm/min. Four specimens of each composition were tested, and the average values were reported. The flexural strength (Q_{fs}) and modulus of elasticity (E_m) were calculated using Eqs. 2 and 3,

$$Q_{fs} = \frac{3PL}{2bd^2} \quad (2)$$

$$E_m = \frac{L^3 m}{4hd^3} \quad (3)$$

where P is the maximum load (N) on the load-deflection curve, L is the support span (63.7 mm), b is the width of beam tested (10 mm), d is the thickness of beam (4 mm), and m is the slope of the tangent to the initial straight-line portion of the load-deflection curve (N/mm of deflection).

Dynamic mechanical thermal analysis (DMTA)

Dynamic mechanical thermal analysis (DMTA) was applied to study the effect of the temperature on the storage modulus ($\log E'$) and loss tangent ($\tan \delta$) of the AN-co-BMA-HNC WPNCs. It is a mechanical test that allows molecules in the wood to interact with mechanical stress. This test was carried out using a Perkin Elmer dynamic mechanical thermal analyser (PE-DMTA, Perkin Elmer, Massachusetts, United States), with a frequency of 10 Hz, strain of x4, and a heating rate of 2 °C/min. The rectangular specimens with moisture contents of about 15% were tested using a dual-cantilever bending mode on a standard bending head. The chamber surrounding the specimen at 65% relative humidity (RH) was cooled by liquid nitrogen. The system provided a simple thermal scan at 2 °C/min with various temperatures ranging from 0 to 200 °C. The glass transition temperature (T_g) was determined from the graph of $\tan \delta$ versus T .

Thermogravimetric analysis (TGA)

The thermogravimetric analysis (TGA) measurements were carried out on 5 to 10 mg of AN-co-BMA-HNC WPNCs at a heating rate of 10 °C/min in a nitrogen atmosphere using a thermogravimetric analyzer (TA Instrument SDT Q600, TA Instruments, Buffalo, New York). The AN-co-BMA-HNC WPNCs were subjected to TGA in high-purity nitrogen under a constant flow rate of 5 mL/min. The thermal decomposition of each sample occurred in a programmed temperature range of 30 to 700 °C. The continuous weight loss and temperature were recorded and analyzed.

Differential scanning calorimetry (DSC) analysis

The AN-co-BMA-HNC WPNCs were analysed using a Perkin Elmer thermal analyser (TGA 8000). All of the measurements were made under a N₂ flow (30 mL/min) with a constant heating rate of 10 °C/min.

Moisture absorption test

The moisture absorption test was carried out using an electronic moisture balance (MOC-120H, Shimadzu Corporation, Kyoto, Japan). The dry wood samples (dried at 25 °C) were immersed in distilled water. The AN-co-BMA-HNC WPNCs were removed and then placed on the pan and weighed. The water absorbed, W_{ab} , was calculated by using Eq. 4,

$$W_{ab} = \frac{W_w - W_d}{W_d} \times 100 \quad (4)$$

where W_{ab} is the absorbed weight (gm), W_w is the weight of the wet WPNCs (gm), and W_d is the weight of the dry WPNCs (gm).

RESULTS AND DISCUSSION

Weight Percent Gain (WPG %)

The values of the WPG for the RW and AN-co-BMA-HNC WPNCs were measured before and after modification and are given in Table 2. The results indicated that the WPG noticeably increased because of the ratios of AN-co-BMA-HNC that reacted well with the hydroxyl groups in the wood fiber (Rahman *et al.* 2013). The AN-co-BMA-HNC polymer matrix aided in removing the impurities from the wood fiber surfaces by using vacuum chamber due to the high pressure of vacuum chamber that left more wood pores within the

wood. AN-co-BMA-HNC was fully copolymerized and fully filled the wood pores, which enhanced the adhesion between the wood fibers and polymer matrix and resulted in a higher WPG. According to the findings, the 50:50 AN-co-BMA-HNC WPNCs had the highest WPG compared with the other monomer systems. This was due to the introduction of 50:50 AN-co-BMA-HNC was fully polymerized which filled up all the pores in the wood cell wall (Gong *et al.* 2012).

Table 2. Average Weight Percent Gain (WPG, %) of the RW and Various Ratios of AN-co-BMA-HNC WPNCs

Samples	Average weight before impregnation (g)	Average weight after impregnation (g)	Weight Percent Gain (WPG, %)
RW	70.756	71.023	0.376
AN-HNC WPNCs	57.880	61.310	5.595
50:50 AN-co-BMA-HNC WPNCs	46.654	56.502	17.429
70:30 AN-co-BMA-HNC WPNCs	62.170	70.924	12.343
BMA-HNC WPNCs	66.488	69.789	4.730

Spectral (FT-IR) Analysis

Figure 1 shows the infrared spectra of the RW and AN-co-BMA-HNC WPNCs.

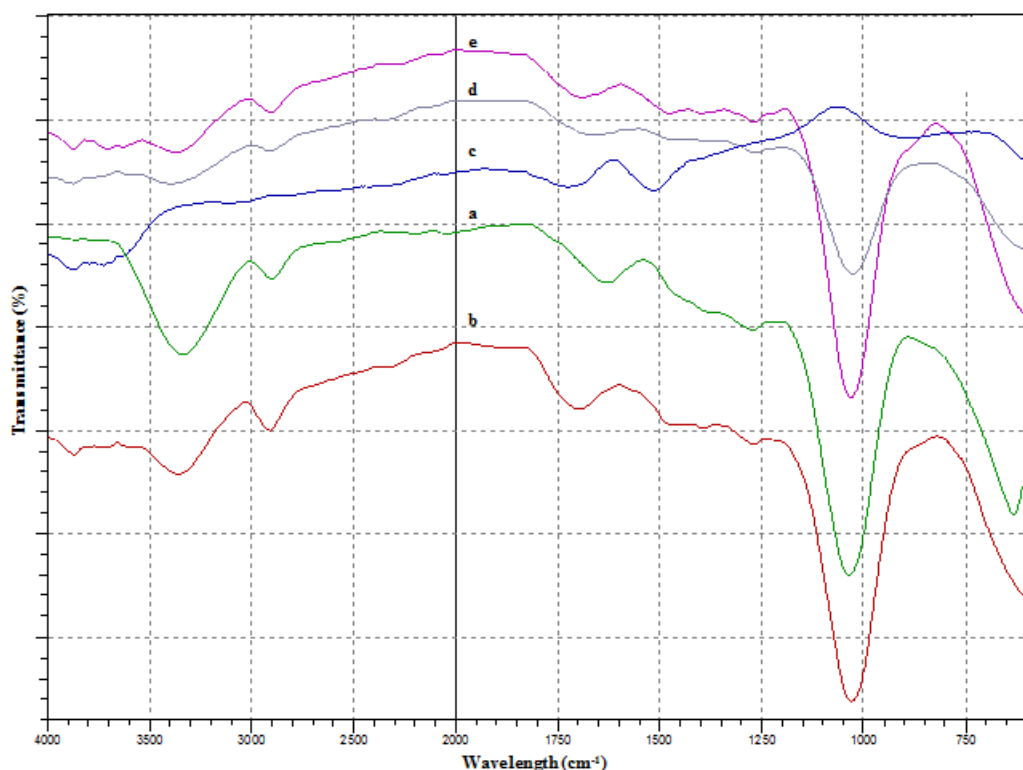
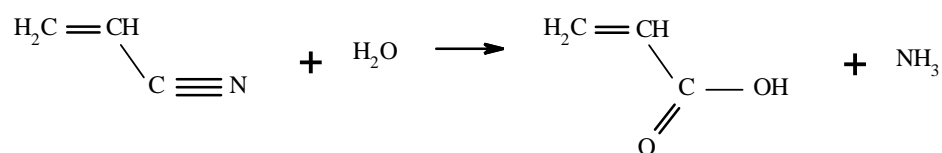


Fig. 1. FT-IR spectra of the (a) RW, (b) AN-HNC WPNCs, (c) 50:50 AN-co-BMA-HNC WPNCs, (d) 70:30 AN-co-BMA-HNC WPNCs, and (e) BMA-HNC WPNCs

From Fig. 1, the RW showed the highest peak intensity at 3300 cm^{-1} compared to the WPNCs. This peak was related to the hydroxyl groups stretching vibration in the wood fiber (Han *et al.* 2010). A specific peak at 2240 cm^{-1} was observed in all of the WPNCs, which was associated with the $-\text{CN}$ groups stretching vibration of acrylonitrile. The peak at about 2360 cm^{-1} was clearly observed, and was attributed to the carbon dioxide absorption band. The high intensity peak at 1745 cm^{-1} was detected in the RW and WPNCs due to the carboxyl groups in the $\text{C}=\text{O}$ stretching vibration (Han *et al.* 2010). The peak at 1200 cm^{-1} was clearly shown in Fig. 1, and was associated with the $\text{C}-\text{O}$ stretching vibration in all of the samples. However, 50:50 AN-co-BMA-HNC WPNCs showed minimal peak intensity at 1200 cm^{-1} due to the strong $\text{C}-\text{O}$ stretching bond after all the polymers were copolymerized. Overall, it was concluded that the AN-co-BMA-HNC was introduced well into the RW by reducing the hydroxyl groups, as well as by forming stronger chemical bonds between the polymer matrix and wood fiber. The 50:50 AN-co-BMA-HNC ratio was the optimum ratio to be impregnated to enhance the RW. The reaction scheme of the AN-co-BMA-HNC with wood fiber is shown in Fig. 2.

Hydrolysis of Acrylonitrile



Reaction of AN-co-BMA-HNC WPNCs

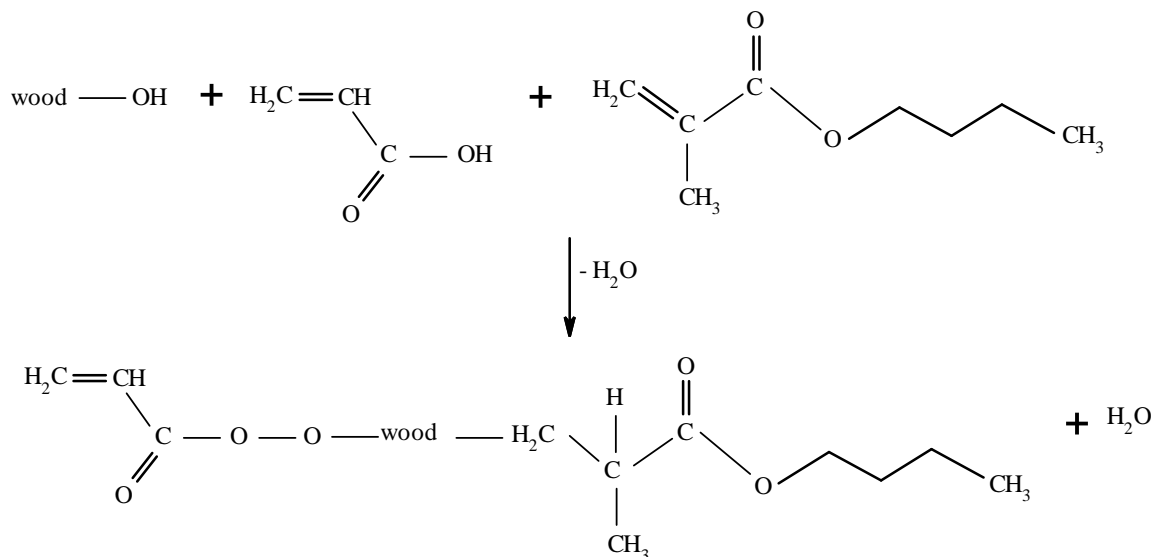


Fig. 2. Proposed schematic reaction diagrams

Scanning Electron Microscopy (SEM) Analysis

The surface morphology of the RW and AN-co-BMA-HNC WPNCs was investigated by SEM, as shown in Fig. 3. Figure 3a shows that the surface of the RW contained a large number of void spaces, which represented the unfilled cell wall and pore volume that absorbed moisture, as reflected in the moisture absorption test (Sultan *et al.* 2016). The AN-HNC WPNCs showed rough and non-uniform wood surfaces, as the AN-

HNC only partially filled the void spaces, as can be seen in Fig. 3b. The void spaces of the RW were filled up by the impregnation of the 50:50 AN-co-BMA-HNC and 70:30 AN-co-BMA-HNC, which provided smoother wood surfaces, as shown in Figs. 3c and 3d.

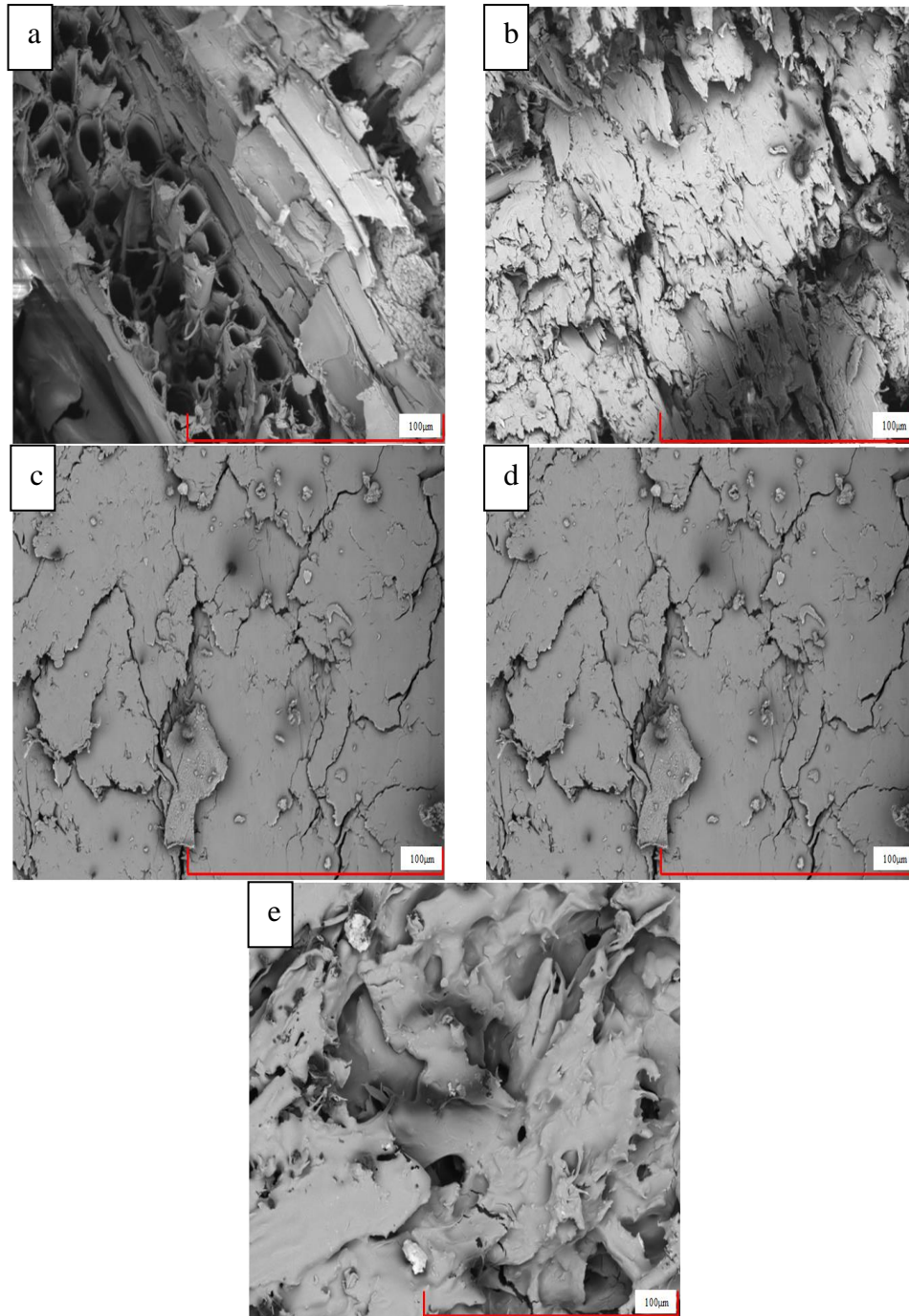


Fig. 3. SEM micrographs of the (a) RW, (b) AN-HNC WPNCs, (c) 50:50 AN-co-BMA-HNC WPNCs, (d) 70:30 AN-co-BMA-HNC WPNCs, and (e) BMA-HNC WPNCs

The addition of the halloysite nanoclay enhanced the impregnation of the AN-co-BMA polymer matrix into the empty pits and capillaries of the wood fiber (Hazarika and Maji 2014). Figure 3e confirms the impregnation of the BMA-HNC into the RW. However,

there were small void spaces detected because of the poor interaction between the polymer matrix and wood fiber (Li *et al.* 2011). The halloysite nanoclay crosslinked with all of the polymer matrix to improve the interaction between the polymer matrix and wood fiber (Sekharnath *et al.* 2015). Therefore, the 50:50 AN-co-BMA-HNC and 70:30 AN-co-BMA-HNC showed better surface morphology, which indicated that they had the stronger interaction between the polymer matrix and wood fiber, as well as the compatibility of polymer matrix impregnation applied in the RW. This was reflected in the thermal and mechanical properties.

Three-Point Flexural Test

Figure 4 shows the flexural properties of the RW and AN-co-BMA-HNC WPNCs. A remarkable increase in the flexural properties was observed when the AN-co-BMA-HNC was impregnated into the RW. This was due to the greater intercalation between the wood fiber and polymer matrix (Khalil *et al.* 2014). The values of the flexural strength of the RW, AN-HNC, 50:50 AN-co-BMA-HNC, 70:30 AN-co-BMA-HNC, and BMA-HNC WPNCs were 0.0053, 0.0653, 0.0950, 0.0668, and 0.0429 GPa, respectively. The good impregnation of the AN-co-BMA-HNC reduced the formation of voids on the wood surface, which enhanced the stress transfer between the polymer matrix and wood fiber (Moodley 2007). With the reduction in void formation, the interaction of the effective cross-sectional area of the wood with the polymer matrix was greatly improved, which resulted in enhanced flexural strength of the WPNCs compared to the RW.

The modulus of elasticity of the RW and AN-co-BMA-HNC WPNCs is presented in Fig. 5. It was shown that the optimum modulus of elasticity was achieved with the 50:50 AN-co-BMA-HNC. This was due to the good intercalation between the AN-co-BMA-HNC and wood fiber, which led to sufficient load transfer and enhanced the modulus of elasticity of the WPNCs compared to the RW (Kuan *et al.* 2004). Also, the small particle size of the AN-co-BMA-HNC had a higher surface area, uniform surface structure, and good dispersion, which provided better adhesion strength to transfer stresses and reduced the elastic deformation from the AN-co-BMA-HNC to wood fiber (Zhang *et al.* 1993). Therefore, it was clearly shown that the 50:50 AN-co-BMA-HNC WPNCs had higher flexural strength and modulus of elasticity compared with the RW and other WPNCs.

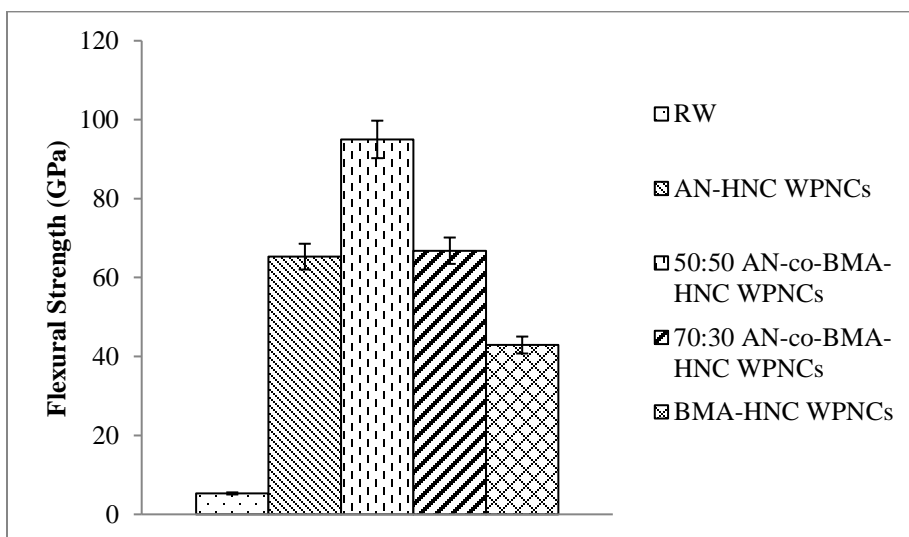


Fig. 4. Flexural strength of the RW and different ratios of AN-co-BMA-HNC WPNCs

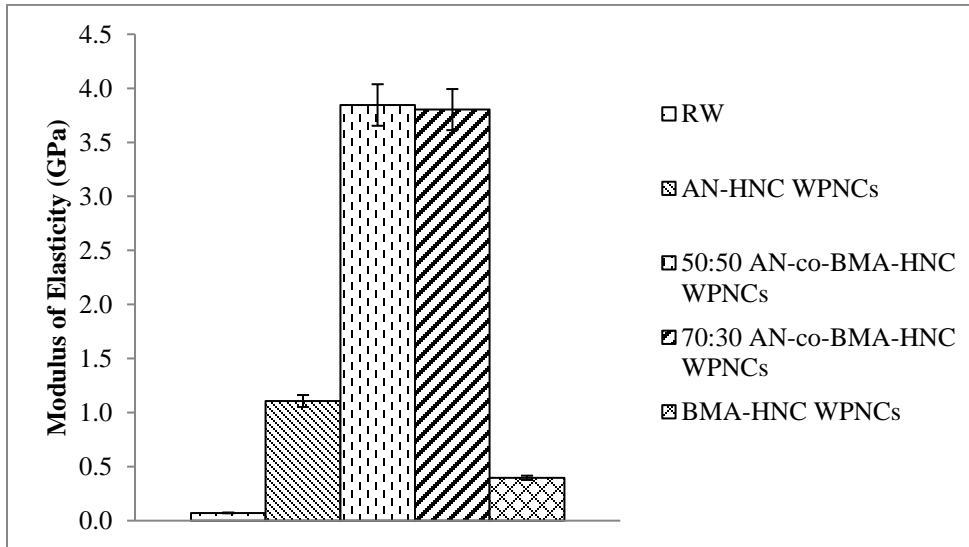


Fig. 5. Modulus of elasticity of the RW and different ratios of AN-co-BMA-HNC WPNCs

Dynamic Mechanical Thermal Analysis (DMTA)

The DMTA properties, such as storage modulus (E'), loss modulus (E''), and loss tangent ($\tan \delta$), were recorded over a temperature range of 30 to 200 °C, as shown in Figs. 6 to 8. The damping property, represented by the $\tan \delta$, was associated with the molecular motions and the bonding between the interface of the polymer matrix and wood fiber (Pashaei and Hosseinzadeh 2016).

The storage moduli of the RW and WPNCs are presented in Fig. 6. The storage moduli of the WPNCs, especially the 50:50 AN-co-BMA-HNC WPNCs, were approximately 58% higher than the storage modulus of the RW. The storage modulus of the WPNCs increased with the addition of polymer matrix, which improved the stiffness of the WPNCs (Pashaei and Hosseinzadeh 2016). The existence of strong interaction between the polymer matrix and wood fiber improved the storage modulus of the WPNCs.

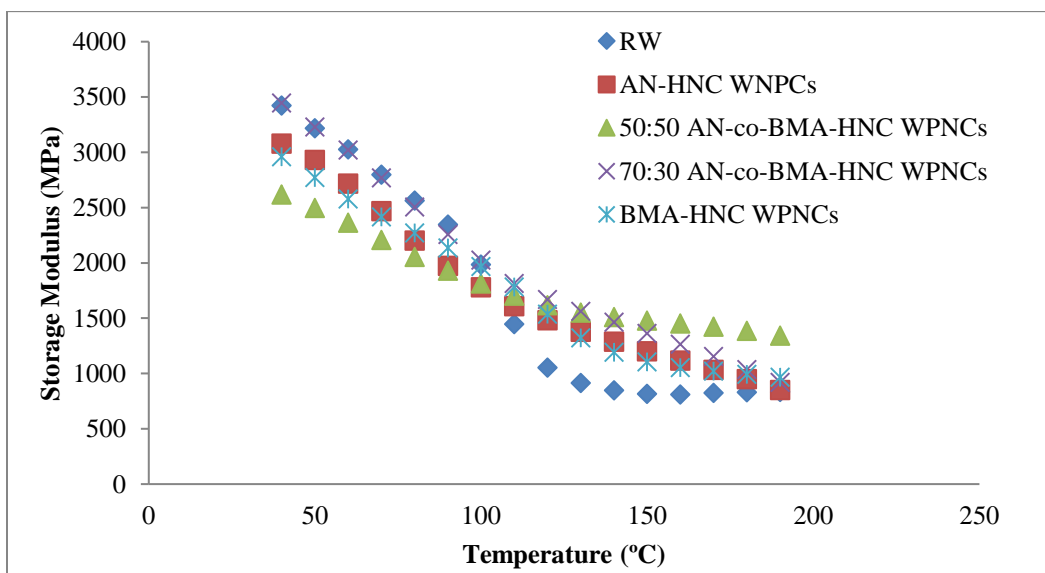


Fig. 6. Storage modulus versus temperature of the RW and different ratios of AN-co-BMA-HNC WPNCs

Figure 7 shows that the 50:50 AN-co-BMA-HNC WPNCs had the highest loss modulus corresponding to the temperature. The polymer chains at the interface were tightly bound, and their mobility was highly restricted (Pashaei and Hosseinzadeh 2016). Thus, larger viscous dissipation occurred more easily, which enhanced the impregnation into the wood fiber and thus improved the interface of the AN-co-BMA-HNC and wood fiber.

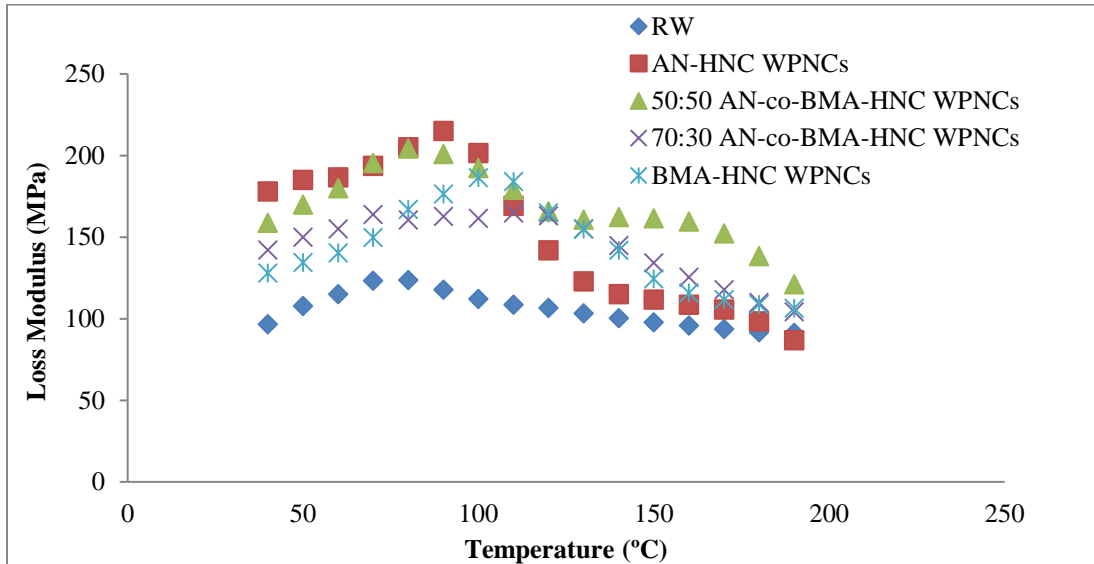


Fig. 7. Loss modulus versus temperature of the RW and different ratios of AN-co-BMA-HNC WPNCs

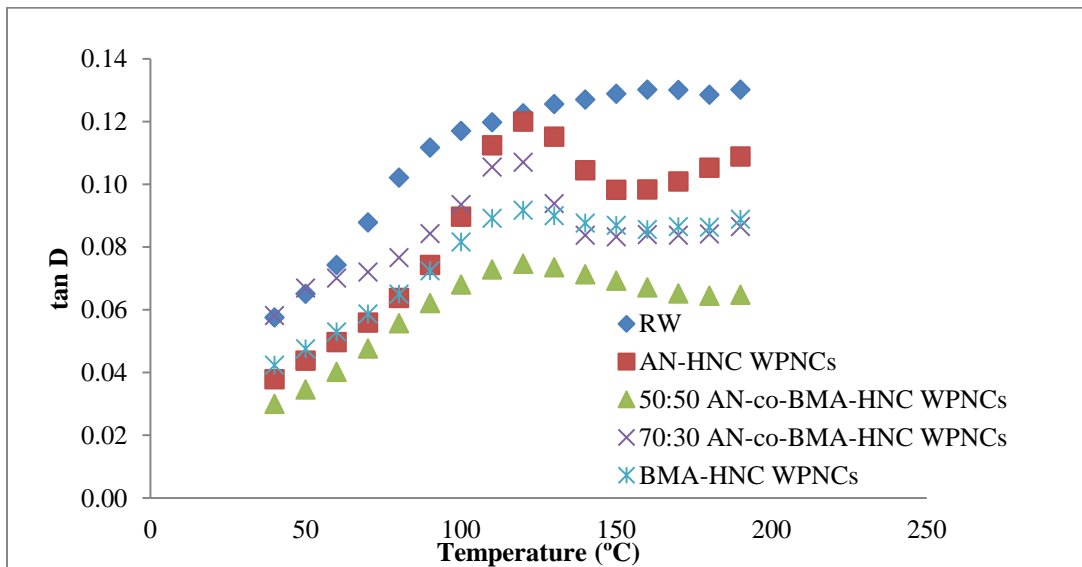


Fig. 8. Tangent δ versus temperature of the RW and different ratios of AN-co-BMA-HNC WPNCs

Figure 8 shows $\tan \delta$ as a function of temperature for the RW and AN-co-BMA-HNC WPNCs. It clearly shows that the impregnation of the AN-co-BMA-HNC into the wood fiber led to lower $\tan \delta$ values compared with the RW. The addition of HNC with polymers shifted the glass transition temperature to a higher value. The 50:50 AN-co-BMA-HNC WPNCs shifted the temperature from 50 to 80 °C, and the peak of the $\tan \delta$ was broader compared with the RW and other WPNCs.

Overall, the storage modulus and loss modulus of WPNCs increased as the loss tangent decreased with the appropriate polymer matrix, as reflected in the three-point flexural test.

Thermogravimetric Analysis (TGA)

The analysis of the thermal stability of the RW and AN-co-BMA-HNC WPNCs was carried out using TGA. There were three steps of weight loss in the AN-co-BMA-HNC WPNCs. The first degradation step, namely vaporization of moisture, occurred at up to 250 °C. This degradation occurred because of the changes in HCN and NH₃ (Bahrami *et al.* 2003). The second degradation step occurred between 250 and 400 °C because of the cyclization and oxidation reactions, as well as the formation of ladder polymer structures in the polyacrylonitrile molecules (Gupta *et al.* 1995). The degradation step around 350 °C was related to the RW or cellulose. The last degradation step started at 400 and went to 600 °C, and this was related to the residues of the RW and WPNCs.

The weight loss in the first step was 3.7 wt.%, 5.5 wt.%, 5.3 wt.%, 5.7 wt.%, and 5.7 wt.% for the RW, AN-HNC, 50:50 AN-co-BMA-HNC-clay, 70:30 AN-co-BMA-HNC-clay, and BMA-HNC WPNCs, respectively. For the second degradation step, the RW, AN-HNC, 50:50 AN-co-BMA-HNC, 70:30 AN-co-BMA-HNC, and BMA-HNC WPNCs had weight losses of 45.2 wt.%, 39.9 wt.%, 39.6 wt.%, 39.5 wt.%, and 39.7 wt.%, respectively. The last degradation step of the RW, AN-HNC, 50:50 AN-co-BMA-HNC, 70:30 AN-co-BMA-HNC, and BMA-HNC WPNCs had weight losses of 13.1 wt.%, 18.8 wt.%, 26.9 wt.%, 22.9 wt.%, and 18.9 wt.%, respectively.

Figure 9 shows that the AN-co-BMA-HNC WPNCs had a higher weight percent loss compared with the RW. This was due to the effect of the acrylate group, which interrupted the nitrile sequence along the acrylonitrile and aided in forming a new chemical bond with butyl methacrylate and halloysite nanoclay (Jamil *et al.* 2014). This bond was linked together in the impregnated wood fiber to enhance the chain mobility of the WPNCs and thus improved the thermal stability of the WPNCs.

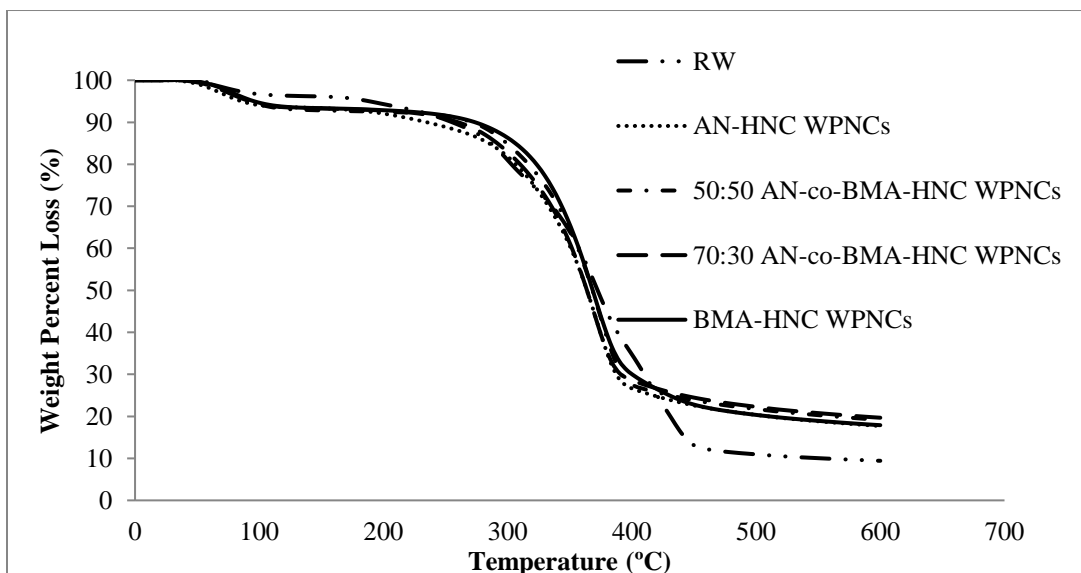


Fig. 9. TGA curves of the RW and different ratios of AN-co-BMA-HNC WPNCs

Table 3 shows the activation energy of the AN-co-BMA-HNC WPNCs using the Arrhenius equation (Chanmal and Jog 2008). The activation energy of the AN-co-BMA-HNC WPNCs was remarkably higher than that of the RW and other WPNCs. The improved thermal stability of the AN-co-BMA-HNC WPNCs can be attributed to the clay, which acts as a compatibilizer that retards the motion of the polymer chain (Benlikaya *et al.* 2009). Apart from that, AN-co-BMA was fully copolymerized with HNC which increased the interfacial bonding strength between the polymers as well as polymers and wood cell wall. Therefore, more activation energy was used to break the strong covalent bonding strength in AN-co-BMA-HNC WPNCs.

Overall, the thermal stability of the AN-co-BMA-HNC WPNCs was higher because of the optimum ratio of the AN-co-BMA-HNC. The impregnation of the AN-co-BMA-HNC into the wood fiber successfully improved the thermal stability of the AN-co-BMA-HNC WPNCs, and this was reflected in the other results.

Table 3. Activation Energy of the RW and Various Ratios of AN-co-BMA-HNC WPNCs Determined by the Arrhenius Equation

Samples	T_i (°C) ^a	T_m (°C) ^b	T_f (°C) ^c	W_{Ti} (%) ^d	W_{Tm} (°C) ^e	W_{Tf} (°C) ^f	Activation Energy (E_a , kJ/mol)
RW	84.0	360.0	456.0	96.3	51.1	13.1	1120.9
AN-HNC WPNCs	96.0	362.0	474.0	94.5	54.6	18.8	1607.6
50:50 AN-co- BMA-HNC WPNCs	97.0	366.0	486.0	94.7	55.1	26.9	2021.1
70:30 AN-co- BMA-HNC WPNCs	97.0	366.0	486.0	94.3	54.8	22.9	1631.9
BMA-HNC WPNCs	96.0	364.0	474.0	94.3	54.6	18.9	1613.2

^a Temperature corresponding to the beginning of decomposition

^b Temperature corresponding to the maximum rate of mass loss

^c Temperature corresponding to the end of decomposition

^d Mass loss at temperature corresponding to the beginning of decomposition

^e Mass loss at temperature corresponding to the maximum rate of mass loss

^f Mass loss at temperature corresponding to the end of decomposition

Differential Scanning Calorimetry (DSC) Analysis

The thermal behaviour of the RW and AN-co-BMA-HNC WPNCs was determined using DSC analysis. The DSC analysis identified the chemical activity that occurred in the wood fiber as the temperature increased (Hamdan *et al.* 2010). The DSC analysis curves of the RW and AN-co-BMA-HNC WPNCs are shown in Fig. 10. The endotherm peaks and enthalpy are shown in Table 4. Both the RW and AN-co-BMA-HNC WPNCs showed broad endotherm peaks between 120 and 160 °C, which are associated with the existence of moisture in the wood. This confirmed that the WPNCs were thermally stable compared

to the RW. Another peak at 210 °C proved the degradation of wood fiber (Akita and Kase 1967).

From Table 4, the crystallization enthalpy of all of the WPNCs was higher than the RW, which proved that the AN-co-BMA-HNC filled wood samples were more crystalline than the RW. This led to better thermal stability in the WPNCs.

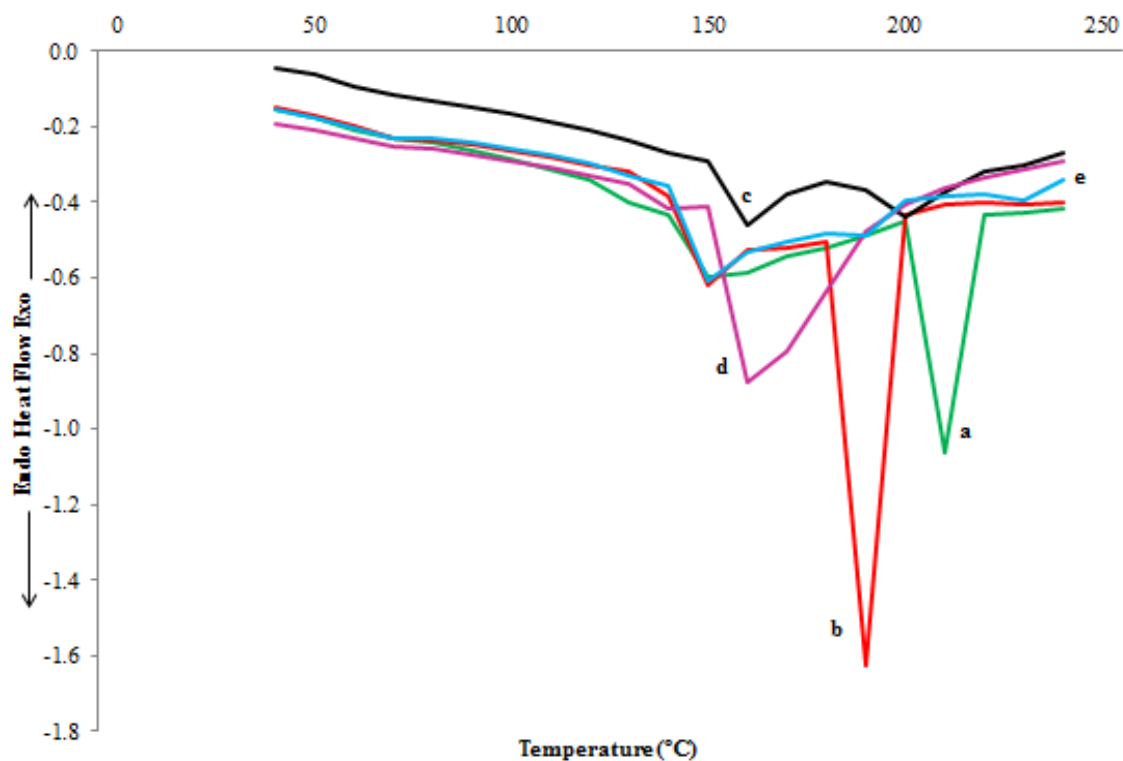


Fig. 10. DSC curves of the (a) RW, (b) AN-HNC WPNCs, (c) 50:50 AN-co-BMA-HNC WPNCs, (d) 70:30 AN-co-BMA-HNC WPNCs, and (e) BMA-HNC WPNCs

Table 4. DSC of the RW and Various Ratios of AN-co-BMA-HNC WPNCs

Samples	Endotherm peaks (°C)	Crystallization Enthalpy (J/g)
RW	139.33	7.64
AN-HNC WPNCs	145.81	21.40
50:50 AN-co-BMA-HNC WPNCs	158.98	59.59
70:30 AN-co-BMA-HNC WPNCs	204.74	42.67
BMA-HNC WPNCs	201.40	41.23

Moisture Absorption Analysis

The moisture absorption characteristics of the AN-co-BMA-HNC WPNCs are presented in Fig. 11. The moisture absorption increased until a certain saturation point as the immersion time increased. The hydrophilic characteristics of the RW acted as a limiting factor in the final application of the WPNCs. The amount of moisture absorbed was

strongly dependent on the molecular structure formed in the WPNCs, which became clearer over the immersion time. The impregnation of the AN-co-BMA-HNC into the RW reduced the amount of moisture absorbed in the WPNCs. This was due to the new chemical bonding between the polar or hydrophilic nature of the lignocellulosic fibers and the hydrophobic nature of the polymer matrix, which aided in reducing the moisture absorbed in all of the WPNCs (Malakani *et al.* 2015). Therefore, the 50:50 AN-co-BMA-HNC WPNCs showed the lowest moisture absorption, followed by the 70:30 AN-co-BMA-HNC WPNCs, BMA-HNC WPNCs, AN-HNC WPNCs, and RW.

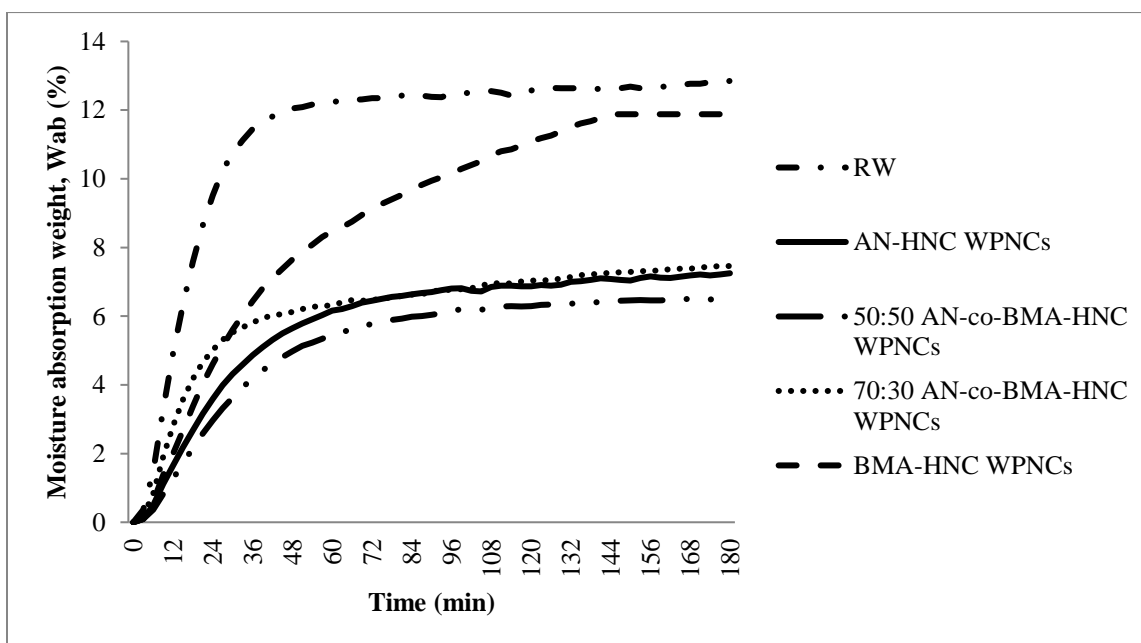


Fig. 11. Moisture absorption curves of the RW and different ratios of AN-co-BMA-HNC WPNCs

CONCLUSIONS

1. In the present study, raw wood (RW) was impregnated with the formulation for acrylonitrile-co-butyl methacrylate/halloysite (AN-co-BMA-HNC) to produce wood-polymer nanocomposites (WPNCs). The physical, mechanical, morphological, and thermal properties of the AN-co-BMA-HNC WPNCs were greatly improved compared with the RW.
2. The 50:50 AN-co-BMA-HNC WPNCs showed the highest weight percent gain with the least hydroxyl groups in the FT-IR spectra.
3. The 50:50 AN-co-BMA-HNC WPNCs provided smoother surface morphology among all of the samples.
4. The 50:50 AN-co-BMA-HNC WPNCs showed the highest flexural strength and modulus of elasticity.
5. The storage modulus and loss modulus of the AN-co-BMA-HNC WPNCs improved greatly with lower $\tan \delta$ compared to the RW.

6. The 50:50 AN-co-BMA-HNC WPNCs exhibited higher thermal stability with noticeably lower moisture absorption.
7. The results proved that the 50:50 AN-co-BMA ratio was the most suitable to be introduced in the RW to form WPNCs.

ACKNOWLEDGMENTS

The authors are grateful for the financial support from the Research and Innovation Management Centre, Universiti Malaysia Sarawak. The grant no. is F02/SpGS/1443/2016/25.

REFERENCES CITED

- Aalaie, J., and Rahmatpour, A. (2007). "Study on preparation and properties of acrylonitrile-butadiene-styrene/montmorillonite nanocomposites," *J. Macromol. Sci. Part B*, 46(6), 1255-1265.
- Akita, K., and Kase, M. (1967). "Determination of kinetic parameters for pyrolysis of cellulose and cellulose treated with ammonium phosphate by differential thermal analysis and thermal gravimetric analysis," *J. Polym. Sci. Pol. Chem.* 5(4), 833-848. DOI: 10.1002/pol.1967.150050411
- Ashori, A. (2008). "Wood-plastic composites as promising green-composites for automotive industries," *Bioresource Technol.* 99(11), 4661-4667. DOI: 10.1016/j.biortech.2007.09.043
- ASTM D 1037, (2012). "Standard test methods for evaluating properties of wood-base fiber and particle panel materials," American Society for Testing and Materials: West Conshohocken, Pa, USA.
- ASTM D 790-03, (2003). "Standard test methods for flexural properties of unreinforced and reinforced plastics and electrical insulating materials," American Society for Testing and Materials: West Conshohocken, Pa, USA.
- Bahrami, S. H., Bajaj, P., and Sen, K. (2003). "Thermal behavior of acrylonitrile carboxylic acid copolymers," *J. Appl. Polym. Sci.* 88(3), 685-698. DOI: 10.1002/app.11637
- Bao, Y., Zhao, W., and Huang, Z. (2013). "Preparation of mesoporous carbons from acrylonitrile-methyl methacrylate copolymer/silica nanocomposites synthesized by *in-situ* emulsion polymerization," *Chinese J. Chem. Eng.* 21(6), 691-697. DOI: 10.1016/S1004-9541(13)60493-1
- Benlikaya, R., Alkan, M., and Kaya, I. (2009). "Preparation and characterization of sepiolite poly(ethyl methacrylate) and poly(2-hydroxyethyl methacrylate) nanocomposites," *Polym. Composite.* 30(11), 1585-1594. DOI: 10.1002/pc.20731
- Bodîrlău, R., Teacă, C. A., and Spiridon, I. (2009). "Preparation and characterization of composites comprising modified hardwood and wood polymers/poly(vinyl chloride)," *BioResources* 4(4), 1285-1304. DOI: 10.15376/biores.4.4.1285-1304
- Chanmal, C. V., and Jog, J. P. (2008). "Dielectric relaxations in PVDF/BaTiO₃ nanocomposites," *eXPRESS Polymer Letters* 2(4), 294-301. DOI: 10.3144/expresspolymlett.2008.35

- Das, A. K., Suin, S., Shrivastava, N. K., Maiti, S., Mishra, J. K., and Khatua B. B. (2014). "Effect of nanoclay on the morphology and properties of acrylonitrile butadiene styrene toughened polyoxymethylene (POM)/clay nanocomposites," *Polym. Compos.* 35(2), 273-282
- Eldin, M. S. M., Elaassar, M. R., Elzatahry, A. A., and Al-Sabah, M. M. B. (2014). "Poly(acrylonitrile-co-methyl methacrylate) nanoparticles: I. Preparation and characterization," *Arab. J. Chem.* DOI: 10.1016/j.arabjc.2014.10.037
- Gong, D. W., Liu, Z. B., Huang, H. W., Zhang, C. Q., and Liang, C. (2012). "Durability of wood-polymer composite prepared by in situ polymerization of functional monomers," *Adv. Mater. Res.* 571, 69-72.
DOI: 10.4028/www.scientific.net/AMR.571.69
- Gupta, A. K., Paliwal, D. K., and Bajaj, P. (1995). "Effect of an acidic comonomer on thermooxidative stabilization of polyacrylonitrile," *J. Appl. Polym. Sci.* 58(7), 1161-1174. DOI: 10.1002/app.1995.070580710
- Hamdan, S., Rahman, M. R., Ahmed, A. S., Talib, Z. A., and Islam, M. S. (2010). "Influence of N,N-dimethylacetamid on the thermal and mechanical properties of polymer-filled wood," *BioResources* 5(4), 2611-2624. DOI: 10.15376/biores.5.4.2611-2624
- Han, N., Zhang, X. -X., and Wang, X. -C. (2010). "Various comonomers in acrylonitrile based copolymers: Effects on thermal behavior," *Iran. Polym. J.* 19(4), 243-253.
- Hazarika, A., and Maji, T. K. (2014). "Modification of softwood by monomers and nanofillers," *Defence Sci. J.* 64(3), 262-272. DOI: 10.14429/dsj.64.7325
- Herrera-Alonso, J. M., Sedlakova, Z., and Marand, E. (2010). "Gas barrier properties of nanocomposites based on *in situ* polymerized poly(*n*-butyl methacrylate) in the presence of surface modified montmorillonite," *J. Membrane Sci.* 349(1-2), 251-257. DOI: 10.1016/j.memsci.2009.11.057
- Jamil, S. N. A. M., Daik, R., and Ahmad, I. (2014). "Synthesis and thermal properties of acrylonitrile/butyl acrylate/fumaronitrile and acrylonitrile/ethyl hexyl acrylate/fumaronitrile terpolymers as a potential precursor for carbon fiber," *Mater.* 7(9), 6207-6223. DOI: 10.3390/ma7096207
- Kallakas, H., Shamim, M. A., Olutubo, T., Poltimäe, T., Süld, T. M., Krumme, A., and Kers, J. (2015). "Effect of chemical modification of wood flour on the mechanical properties of wood-plastic composites," *Agronomy Res.* 13(3), 639-653.
- Khalil, H. P. S. A., Jawaid, M., Firoozian, P., Alothman, O. Y., Paridah, M. T., and Zainudin, E. S. (2014). "Flexural properties of activated carbon filled epoxy nanocomposites," *Malays. J. Anal. Sci.* 18(2), 391-397.
- Kobayashi, M., Rharbi, Y., Brauge, L., Cao, L., and Winnik, M. A. (2002). "Effect of silica as fillers on polymer interdiffusion in poly(butyl methacrylate) latex films," *Macromolecules* 35(19), 7387-7399. DOI: 10.1021/ma0115951
- Kuan, H. -C., Ma, C. -C. M., Chen, K. H., and Chen, S. -M. (2004). "Preparation, electrical, mechanical and thermal properties of composite bipolar plate for a fuel cell," *J. Power Sources* 134(1), 7-17. DOI: 10.1016/j.powsour.2004.02.024
- Larsen, K., Larsen, S. S., and Vidal, J. E. (1984). *Flora of Thailand Volume Four Part One*, TISTR Press, Bangkok, Thailand.
- Li, Y. -F., Liu, Y. -X., Wang, X. -M., Wu, Q. -L., Yu, H. -P., and Li, J. (2011). "Wood-polymer composites prepared by *in situ* polymerization of monomers within wood," *J. Appl. Polym. Sci.* 119(6), 3207-3216. DOI: 10.1002/app.32837

- Malakani, M., Bazyar, B., Talaiepour, M., Hemmasi, A. H., and Ghasemi, I. (2015). "Effect of acetylation of wood flour and MAPP content during compounding on physical properties, decay resistance, contact angle, and morphology of polypropylene/wood flour composites," *BioResources* 10(2), 2113-2129. DOI: 10.15376/biores.10.2.2113-2129
- Mekhmer, W. K., El-Ala, A. A. A., and El-Rafey, E. (2006). "Clay as a filler in the thermoplastic compounding," *Mol. Cryst. Liq. Cryst. A* 354(1), 13-21. DOI: 10.1080/10587250008023597
- Moodley, V. K. (2007). *The Synthesis, Structure and Properties of Polypropylene Nanocomposites*, Master's thesis, Durban Univ. of Technol., Durban, South Africa.
- Pakeyangkoon, P., and Ploydee, B. (2013). "Mechanical properties of acrylate-styrene acrylonitrile/bagasse composites," *Advanced Materials Research* 747, 355-358. DOI: 10.4028/www.scientific.net/AMR.747.355
- Pashaei, S., and Hosseinzadeh, S. (2016). "Preparation of organo nanoclay incorporated polyamide/melamine cyanurate/nanoclay composites and study on thermal and mechanical behaviours," *Iran. Chem. Comm.* 4(1), 102-114.
- Prochoń, M., Przepiórkowska, A., and Zaborski, M. (2007). "Keratin as a filler for carboxylated acrylonitrile-butadiene rubber XNBR," *J. Appl. Polym. Sci.* 106(6), 3674-3687. DOI: 10.1002/app.26324
- Rahman, M. R., Lai, J. C. H., Hamdan, S., Ahmed, A. S., Bains, R., and Saleh, S. F. (2013). "Combined styrene/MMA/nanoclay cross-linker effect on wood-polymer composites (WPCs)," *BioResources* 8(3), 4227-4237. DOI: 10.15376/biores.8.3.4227-4237
- Sekharnath, K. V., Rao, S. J., Maruthi, Y., Babu, P. K., Rao, K. C., and Subha, M. C. S. (2015). "Halloysite nanoclay-filled blend membranes of sodium carboxyl methyl cellulose/hydroxyl propyl cellulose for pervaporation separation of water-isopropanol mixtures," *Ind. J. Adv. Chem. Sci.* 3(2), 160-170.
- Shishavan, S. M., Azdast, T., and Ahmadi, S. R. (2014). "Investigation of the effect of nanoclay and processing parameters on the tensile strength and hardness of injection molded acrylonitrile butadiene styrene-organoclay nanocomposites," *Mater. Des.* 58, 527-534.
- Siddiqui, M. N., Redhwi, H. H., Gkinis, K., and Achilias, D. S. (2013). "Synthesis and characterization of novel nanocomposite materials based on poly(styrene-co-butyl methacrylate) copolymers and organomodified clay," *Eur. Polym. J.* 49(2), 353-365. DOI: 10.1016/j.eurpolymj.2012.10.022
- Singh, P., and Ghosh, A. K. (2014). "Torsional, tensile and structural properties of acrylonitrile-butadiene-styrene clay nanocomposites," *Mater. Design* 55, 137-145. DOI: 10.1016/j.matdes.2013.09.036
- Stark, N. M., and Matuana, L. M. (2007). "Characterization of weathered wood-plastic composite surfaces using FTIR spectroscopy, contact angle, and XPS," *Polym. Degrad. Stabil.* 92(10), 1883-1890. DOI: 10.1016/j.polymdegradstab.2007.06.017
- Sultan, M. T., Rahman, M. R., Hamdan, S., Lai, J. C. H., and Talib, Z. A. (2016). "Clay dispersed styrene-co-glycidyl methacrylate impregnated kumpang wood polymer nanocomposites: Impact on mechanical and morphological properties," *BioResources* 11(3), 6649-6662. DOI: 10.15376/biores.11.3.6649-6662
- Těšinova, P. (2011). *Advances in Composite Materials – Analysis of Natural and Man-Made Material*, InTech, Rijeka, Croatia.

- Vorreiter, L. (1949). *Holztechnologien Handbuch. Band 1: Allgemeines, Holzkunde, Holzschutz and Holzverwertung*, Verlag Georg Fromme und Co., Vienna, Austria.
- Zhang, M., Zeng, H., Zhang, L., Lin, G., and Li, R. K. Y. (1993). "Fracture characteristics of discontinuous carbon fibre-reinforced PPS and PES-C composites," *Polym. Polym. Compos.* 1(5), 357-365.

Article submitted: October 16, 2016; Peer review completed: December 4, 2016; Revised version received: January 19, 2017; Accepted: Jan. 20, 2017; Published: January 26, 2017.

DOI: 10.15376/biores.12.1.1871-1889